Prediction of Noise and Interference Cancellation With a Moving Compact Receiver Array in an Indoor Environment

Hendrik Rogier, *Member, IEEE,* and Daniël De Zutter, *Fellow, IEEE*

***Abstract*—An interference and noise cancellation technique based on a reference signal is studied for a compact receiver antenna array placed in an indoor environment. The exact active element pattern method is used to model the radiation characteristics of the array, including mutual coupling between the antenna elements. A two-dimensional ray-tracing technique describes the signal propagation in the indoor environment for a moving receiving antenna.**

***Index Terms*—Adaptive arrays, antenna array mutual coupling, shaped beam antennas, ultrahigh-frequency (UHF) radio propagation.**

I. Introduction

SYSTEMS for personal communications, such as Bluetooth, HiperLAN, and IEEE 802.11, which operate over small distances (10–100 m) in an indoor environment are under full development and will become increasingly important in the near future. The propagation of signals in an indoor environment (picocells) [1]–[5] differs substantially from signal propagation in rural and urban areas (macrocells and microcells) [6]. In picocells, signals arrive at the receiver following a large number of different paths, whereas in microcells and macrocells only a few dominant angles of arrival need to be considered. Moreover, time delays between copies of the signal arriving from different paths are most often negligible in the indoor environment for bit rates up to 2 Mb/s [7]. In urban and rural areas, on the other hand, these delays can become significant due to scattering at distant buildings, hills, and other large objects. Both prior observations show that care must be taken when applying smart antenna algorithms, typically used in microcells and macrocells, to antenna configurations in indoor environments. Indeed, many adaptive algorithms for array steering assume that the desired signal reaches the antenna array along one dominant angle of arrival (AoA), while interfering signals arrive at the receiving array along directions, clearly distinguishable from the desired AoA. Because the latter is not necessarily the case in an indoor environment, only a small number of systems for such environments have been proposed in the literature [8]. Keeping this in mind, modeling tools describing the typical channel characteristics can be of great help in understanding the behavior of adaptive beamforming algorithms and in predicting their performance in realistic indoor environments.

In this paper, a two-dimensional (2-D) ray tracer is used for modeling the picocell environment. The ray-tracing technique has been applied for signal prediction in indoor environments for a long time [9]. Since an approximate model for the environment is sufficient for this feasibility study, we chose not to incorporate more advanced features that are already described in literature, e.g., three-dimensional (3-D) propagation [10]; [11]; diffraction effects; and detailed material descriptions of walls [12], windows [13], and furniture [14]. Instead, we chose to incorporate the movement of the receiver in our ray tracer, including Doppler shift [15], and changing ray parameters with time. To this end, we do not only calculate all the relevant ray parameters, but also their derivatives with respect to the movement of the receiver. This information is used to construct a table describing the time history of all the rays. This table combined with the derivative information allows accurate interpolation with respect to time for each separate ray. We believe that this approach is new to the literature.

A second important issue that is relevant to the application of smart antenna algorithms in indoor environments involves the antenna arrays that can be installed on mobile devices. Inevitably, these must remain sufficiently small to allow easy integration. This, of course, results in a reduction of the size of the antenna elements and their spacing and, thus, in an increase in the mutual coupling between elements. Many algorithms for adaptive antennas are based on the assumption of a perfect array in which the antenna elements are equispaced and exhibit no mutual coupling. It is clear that, in order to be able to use the compact array without deterioration of the performance of the smart antenna system, a suitable adaptive algorithm must be chosen that can both handle the mutual coupling of the antenna elements and the severe multipath behavior of the indoor environment.

In summary, we can state the goal of this paper as follows: to investigate the possible use of smart antenna algorithms in indoor environments, given an omnidirectional source at the transmitter end and a compact array at the receiver end by using a 2-D ray-tracing approach to describe the channel characteristics of the indoor environment. We hereby assume that the receiver is moving around in the indoor environment at a constant speed. In Section II, a brief summary of the modeling approach is given, presenting the main features of the 2-D ray-tracing method and

Manuscript received July 26, 2002; revised April 7, 2003 and September 8, 2004. The research of H. Rogier was supported by a Grant from the Mobile Multimedia Communication Systems and Networks (DWTC/SSTC MOTION) project. He is a Postdoctoral Research Fellow of the Fund for Scientific Research, Flanders (FWO-V).

The authors are with the Information Technology Department, Ghent University, Ghent B-9000, Belgium (e-mail: hendrik.rogier@intec.UGent.be; daniel.dezutter@intec.UGent.be).

Digital Object Identifier 10.1109/TVT.2004.838885

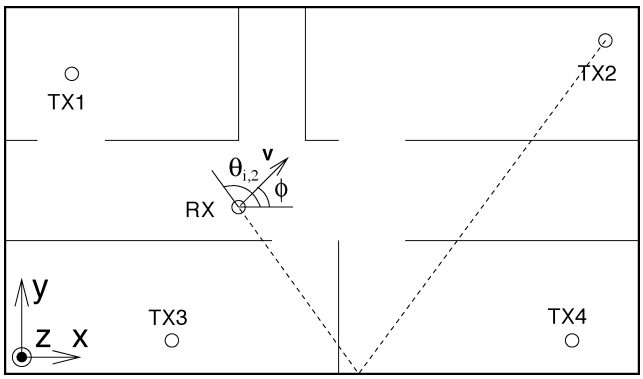

Fig. 1. Receiver moving in an indoor environment.

the active element pattern technique to model the array placed on the mobile receiver. In Section III, we apply both techniques to model a compact HiperLAN array placed in a picocell environment. We try to detect the bit sequence emitted by the desired source in the presence of an interferer plus noise. Both least-squares (LS) based training and tracking techniques are considered for steering the array at the mobile side.

II. Overview of the Modeling Approach

Consider a moving receiver placed in a 2-D indoor environment in the presence of K omnidirectional sources emitting band-limited signals around a central frequency f_c, as illustrated in Fig. 1. The electric field emitted by these sources is polarized along the vertical z-direction. Our aim now is to detect, at a given receiver, a signal arriving from a desired transmitter in the presence of noise and interfering sources. The receiver moves through the indoor environment with a constant speed $\mathbf{v} = v(\cos\phi\mathbf{u}_x + \sin\phi\mathbf{u}_y)$. Due to the nature of the picocell environment, for each source a large number of multipaths will arrive at the receiver, e.g., a mobile terminal. Assume that the receiver consists of a compact antenna array with important mutual coupling between the antenna elements. Due to the limited amount of space available at the receiver, this array consists only of a few elements. The question then arises if such an array can still be used for adaptive beamsteering purposes while the receiver moves and is as such submitted to the rapid field changes that occur in a typical indoor environment. Another important aspect when deploying compact arrays in wireless systems relates to the diversity gain when applying diversity combining. For small antenna-element spacings, it is well known that the diversity gain drastically decreases due to increasing antenna element correlation.

A. Modeling of the Compact Array and the Signal Detected by That Array

Suppose that the antenna array consists of M elements (e.g., $M = 4$ in the compact HiperLAN patch array of Fig. 4, which will be discussed in Section III). The close spacing of the antenna patches does not allow to apply the classical simple array theory to straightforwardly combine the fields of the separate antenna elements. However, it is shown in [16] that the exact active element pattern method can be used to rigorously model the behavior of such an array and to perform beamsteering. For an incoming plane wave or, in the high-frequency limit, a ray impinging on the array along an AoA $\theta_{i,k}(t)$ at time t, the open-circuit voltage at terminals of antenna element $m(m = 1, 2, \ldots, M)$ is given by

$$v_{m(t)}^{i,k} = \alpha_m \mathbf{E}_{\text{inc}}\big(t, \theta_{i,k}(t)\big)(\mathbf{r} = 0).\mathbf{F}_m(\theta_{i,k}). \tag{1}$$

In (1), $\theta_{i,k}(t)$ represents the AoA of ray i originating from transmitter k. $\mathbf{F}_m$ represents the so-called active element pattern of the array when exciting terminal m. Details on how to determine F_m, properly taking into account all mutual coupling effects between the array elements, are to be found in [16]. $\mathbf{E}_{\text{inc}}$ represents the incoming field at a phase reference location $\mathbf{r} = 0$ (located somewhere on the array) while calculating $\mathbf{F}_m$. Finally, α_m is a proper weighting factor between the field quantities and the open-circuit voltage at element m. We again refer to [16] for more details. It is important at this point to remark that, in absence of mutual coupling, the active element patterns $\mathbf{F}_m$ of each array element will only differ by a phase factor. However, in this contribution the $\mathbf{F}_m$'s of the different elements will differ in amplitude, phase, and polarization, due to the mutual coupling. This restricts the beamforming freedom of the array and raises the question, discussed in the remainder of this paper, whether the remaining beamsteering capabilities remain sufficient for the receiver to track the desired transmitter.

Since all sources are vertically polarized, the complex envelope $v_{m(t)}$ of the total signal picked up at the receiver at element m of the array is, therefore, given by

$$v_m(t) = \alpha_m \sum_{k=1}^{K} \sum_{i=1}^{N_k} F_{z,m}\big(\theta_{i,k}(t)\big) A_{i,k}(t) u_k\big(t, \tau_{i,k}(t)\big) e^{j\omega_{d,i,k}(t)t}. \tag{2}$$

The sum extends over $N = \sum_{k=1}^{K} N_k$ rays that reach the receiver. $A_{i,k}$ represents the complex path loss at frequency f_c and $\tau_{i,k}(t)$ represents the delay of ray i traveling from transmitter k toward the receiver. $F_{z,m}$ represents the z-component of F_m and $u_k(t)$ represents the modulated signal emitted by transmitter k. $\omega_{d,i,k}(t) = -2\pi f(v/c)\cos(\theta_{i,k}(t) - \phi)$ represents the Doppler shift for ray i when the receiver is moving with speed $v(v \ll c)$ along the direction given by the angle ϕ. Note that, because of the movement of the receiver, the path loss, delay, and AoA of the rays are all time dependent. In order to limit complications, however, we will assume that the frequency band of the band-limited signal is sufficiently small so that the ray characteristics as well as the array response remain constant throughout the frequency band.

To derive the channel model in practice, an image-based ray-tracing approach is used, which takes into account up to fourth-order reflections. Walls and objects in the indoor environment are modeled as dielectrics, with reflection and transmission taken into account. To account for the movement of the receiver, a number of field sample points are registered along the direction of movement. At each point, all rays together with their characteristics are recorded. In order to derive the received signal $v_m(t)$ at an arbitrary time instant t by means of (2), the ray characteristics $\theta_{i,k}(t)$, $A_{i,k}(t)$, $\tau_{i,k}(t)$, and $\omega_{d,i,k}(t)$ are required at the correct continuous time instance. To implement an accurate interpolation scheme in time, the

TABLE I
INTERPOLATION TABLE FOR THE AOA AS A FUNCTION OF TIME

t_1	t_2	$\dots$	t_l	t_{l+1}	$\dots$	$t_{l'}$	$t_{l'+1}$	$\dots$	t_L
$\theta_{1,k}(t_1)$	$\theta_{1,k}(t_2)$	$\dots$	$\theta_{1,k}(t_l)$	$\theta_{1,k}(t_{l+1})$	$\dots$	$\theta_{1,k}(t'_l)$	$\theta_{1,k}(t_{l'+1})$	$\dots$	$\theta_{1,k}(t_L)$
$\theta_{2,k}(t_1)$	$\theta_{2,k}(t_2)$	$\dots$	$\theta_{2,k}(t_l)$	0	$\dots$	0	0	$\dots$	0
$\vdots$	$\vdots$	$\vdots$	$\vdots$	$\vdots$	$\vdots$	$\vdots$	$\vdots$	$\vdots$	$\vdots$
0	0	$\dots$	0	0	$\dots$	0	$\theta_{i,k}(t_{l'+1})$	$\dots$	$\theta_{i,k}(t_L)$
$\vdots$	$\vdots$	$\vdots$	$\vdots$	$\vdots$	$\vdots$	$\vdots$	$\vdots$	$\vdots$	$\vdots$
0	0	$\dots$	0	$\theta_{N_k,k}(t_{l+1})$	$\dots$	$\theta_{N_k,k}(t_{l'})$	0	$\dots$	0

derivatives with respect to the movement of the receiver are also calculated for these ray parameters. While moving from one sample point to the next, an interpolation table is constructed that keeps track of all the different rays as a function of time. Each ray at the new sample point is either the continuation of a ray existing at the previous sample point or is a new ray emerging at that point. Which of the two possibilities actually occurs is determined by evaluating the derivative of the AoA with respect to time and using a Taylor series at the previous sample point to estimate the AoA at the new sample point. This results in a table of the form schematically shown in Table I. Each entry in the table tracks the AoA of a ray as a function of time. The time instants $t_1, t_2, \dots, t_L$ correspond to the position of the moving receiver at the consecutive sample points. One particular ray can be present during the whole time (e.g., ray $\theta_{1,k}$ of Table I) or can emerge at a certain time instance (e.g., ray $\theta_{i,k}$ of Table I) and/or disappear at a certain time (e.g., ray $\theta_{N,k}$ of Table I). Besides the AoA information, the ray characteristics $A_{i,k}(t)$, $\tau_{i,k}(t)$, and $\omega_{d,i,k}(t)$ are recorded in similar tables. In order to find each individual ray contribution at a given time t, an interpolation scheme is applied, making use of the tables containing the ray characteristics and their derivatives with respect to the movement.

Combining the active element pattern method for the receiver array, the propagation channel description through ray tracing and the time-domain interpolation, we are now armed with complete detailed information (2) about the signals detected by the elements of the receiver array as a continuous function of time t. This will enable us to set up a training scheme for detection and tracking of a desired transmitter.

B. Training the Receiver for Detection and Tracking of the Desired Transmitter

Assume that each transmitter emits a pseudorandom binary phase-shift keying (BPSK) modulated bit stream $u_k(t)$ with the same bit rate $f_b = (1/(T_b)$ and at the same carrier frequency f_c. The bit rate is chosen such that $T_b \gg \max_{i,k}(\tau_{i,k})$, i.e., the duration of each bit is much larger than the maximum propagation delay encountered between transmitter and receiver. An omnidirectional antenna at the receiver will detect the sum of the wanted signal and interfering signals. Hence, unless the wanted signal is considerably stronger than the interfering signals, the receiver will not be able to decode the desired bit stream. Let us now examine whether a directional antenna can detect the wanted signal in the presence of interfering sources that emit at the same frequency. The output signal of the antenna array at the receiver is given by

$$y(t) = \sum_{m=1}^{M} w_m(t) x_m(t) \tag{3}$$

with $w_m(t)$ being a complex weight applied at the mth antenna element. We assume that the signal $x_m(t) = v_m(t) + n_m(t)$ received at the mth antenna element is the sum of the open-circuit voltage $v_m(t)$, given by (2), and an additive white Gaussian noise (AWGN) component $n_m(t)$ with noise power σ_n^2. The signal-to-noise ratio (SNR) at the output of the array is defined as

$$\text{SNR} = \frac{|\overline{v}|^2}{\sigma_n^2} \tag{4}$$

where $|\overline{v}|^2$ represents the average power of the input signals $v_m(t)$, the average being taken over all array elements m and over the complete bit sequence under consideration.

Let us, by way of example, assume that the first 16 bits $s_1, s_2, \dots, s_{16}$ of the desired bit sequence are known to the receiver. These bits can then be used as a training sequence to determine the array weights of the antenna array, by solving the following matrix system in the least-square sense:

$$\begin{cases} w_1(t_{17})x_1(t_1) + w_2(t_{17})x_2(t_1) \\ \quad + \dots + w_M(t_{17})x_M(t_1) = s_1 \\ \vdots \qquad\qquad\qquad\qquad \vdots \\ w_1(t_{17})x_1(t_{16}) + w_2(t_{17})x_2(t_{16}) \\ \quad + \dots + w_M(t_{17})x_M(t_{16}) = s_{16} \end{cases} \tag{5}$$

with $t_j = (j - (1/2))T_b$, $j = 1, \dots, 16$. In (5), the weights $w_m(t_{17})$ are determined at time instance $t_{17} = 16T_b + (T_b/2)$. They are then used to decode the first unknown bit arriving at time instance t_{17}.

After training the receiving antenna array, the desired signal is tracked based on the estimated bit sequence, given the estimates $\hat{y}_i = y((i-(1/2))T_b)$ corresponding to the desired bit sequence s_i. Before detecting the jth bit, the 16 prior estimates are used

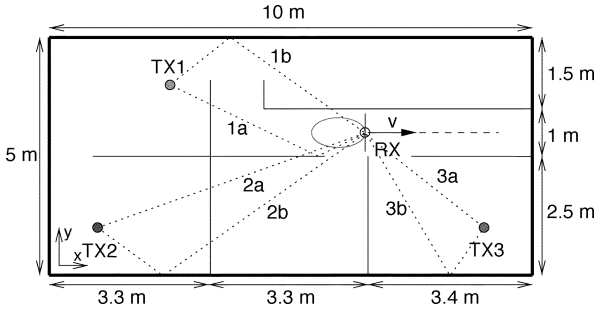

Fig. 2. Simple office environment.

to update the array weights at time instant t_j by solving a matrix system similar to (5) in the LS sense as

$$\begin{cases} w_1(t_j)x_1(t_{j-16}) + w_2(t_j)x_2(t_{j-16}) \\ \quad + \ldots + w_M(t_j)x_M(t_{j-16}) = \hat{y}_{j-16} \\ \vdots \qquad\qquad\qquad\qquad\qquad \vdots \\ w_1(t_j)x_1(t_{j-1}) + w_2(t_j)x_2(t_{j-1}) \\ \quad + \ldots + w_M(t_j)x_M(t_{j-1}) = \hat{y}_{j-1} \end{cases} \tag{6}$$

with $t_j = \big(j - (1/2)\big)T_b$, $j = 1, \ldots, 16$.

III. Example: A Compact Array for the HiperLAN Protocol

To illustrate our technique, we consider a simple 10×5-m office environment shown in Fig. 2. The exterior walls have a thickness of 30 cm and are modeled as dielectrics slabs with $\epsilon_r = 3.5 - 0.3j$. The inner walls have a thickness of 10 cm and are assumed to be of lighter construction, characterized by $\epsilon_r = 2 - 0.1j$. Three sources are present, emitting pseudorandom bit sequences with bit rate $f_b = 100$ kb/s at a carrier frequency of $f_c = 5.25$ GHz. In Fig. 3, the AoAs and relative amplitude of each ray are shown for the different transmitter–receiver configurations and for the receiver located at the position ($x = 6.54$ m, $y = 3$ m), shown in Fig. 2. Clearly, a large number of multipath components exist for all transmitter–receiver combinations. For each transmitter–receiver combination, the most important ray contributions are shown in Fig. 2. Only TX3 [$x = 9$ m $y = 1$ m, Fig. 3(c)] generates a dominant line-of-sight (LoS) component at the receiver. The LoS components from TX1 [$x = 2.5$ m $y = 4$ m, Fig. 3(c)] and TX2 [$x = 1$ m $y = 1$ m, Fig. 3(c)] are blocked by the inner walls.

Let us first assume an omnidirectional antenna at the receiver. Since the maximum delay for the configuration under study is 120 ns, it is safe to assume that delays are negligible when working with a bit rate of $f_b = 100$ kb/s. Now consider one transmitter emitting a desired signal while another at the same time emits an interfering signal at the same carrier frequency. The receiver moves at a constant speed of 1 m/s along the x-direction. The location of the receiver shown in Fig. 2 corresponds to $t = 0$. When TX1 emits the desired 400-b pseudorandom sequence whereas TX2 or TX3 is emitting an interfering 400-b pseudorandom sequence, the receiver picks up signals coming from both the desired and interfering transmitter, resulting in an average bit-error rate (BER) of ≈ 0.5 (for one particular pseudorandom sequence, 192 bit errors when TX2 is interfering and 194 bit error when TX3 is the interferer).

Next, we place an array at the receiver and try to find out whether a steerable array can succeed in reducing the BER. The example array, shown in Fig. 4, consists of four planar single feed microstrip rectangular ring antennas designed to operate in the 5.15–5.35-GHz HiperLAN band. The complete array fits into a rectangle of 93.3 mm$\times$17.46 mm. More details about the antenna elements can be found in [17]. The characteristics of the complete array are simulated by means of the full-wave simulator Momentum (Agilent Technologies, Palo Alto, CA). The broadside direction of the planar array is oriented along the negative x-axis.

A. Effect of Using a Single Training Sequence

We again consider different transmitter/interferer–receiver combinations emitting 400-b pseudorandom sequences and use the first 16 b of the desired signal as a *training sequence* known to the receiver to calculate the four array weights. The received signal $\mathrm{Re}[y(t)]$ (3) after training no longer exhibits bit errors, neither for TX1 emitting the desired signal and TX2 being the interferer nor for TX3 emitting the desired signal and TX1 being the interferer. In Fig. 5, the signal-to-interference ratio (SIR) in decibels (defined as the ratio of the received power of the desired signal to the received power of the interfering signal) is shown for different combinations of transmitters emitting the desired and interfering signals. When TX1 is the desired receiver and TX3 the interferer, the SIR remains high for a long period of time after training the array, since the array points toward TX1 whereas TX3 is located at the back side of the array and the LoS component of TX3 is suppressed. When TX3 is desired and TX1 is interfering, the interference cancellation can only be achieved by a subtle phase equilibrium and the SIR rapidly decreases after training, as constructive interference of the ray contributions coming from TX3 and destructive interference of the contributions emitted by TX1 disappear because of movement.

To better illustrate this effect, in Fig. 6 we consider the AoA of the desired and interfering signal as well as the radiation pattern of the receiving array, just after the training period. Since the AoA of both the desired and interfering signal are widely distributed, the interference cancellation clearly does not work by placing nulls in the direction of all dominant AoA of the interfering signal. Instead, interference is suppressed by adjusting the phase of the different components of the interfering signal. The components of the desired transmitter add up to yield a unit response while the components of the interfering transmitter cancel out. Even for a small movement of the receiver, phase changes in the ray contributions will tend to destroy the delicate phase- and amplitude-based interference cancellation in the array. Hence, the question clearly arises whether the moving array will be capable of adjusting after the training period. At this point, it also becomes obvious that one should carefully construct the ray histories as a function of time, as we did through our tabulation and interpolation technique explained before.

When white Gaussian noise is added at each branch of the receiver with a SNR $= 10$ dB, the array remains able to detect desired bit sequences coming from transmitter TX1 (and TX2) in the presence of interferer TX3, after training the array with a 16-b training sequence. However, because of the deterioration of

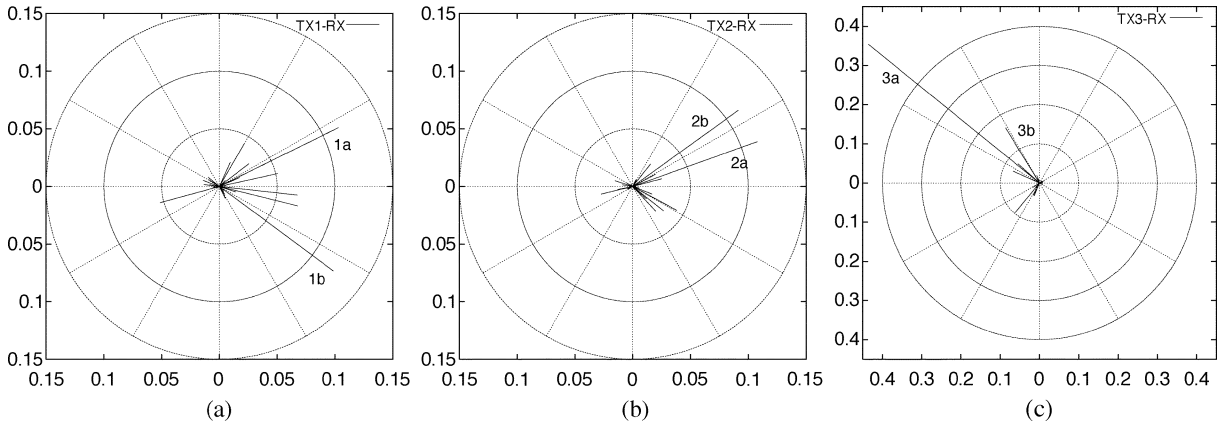

Fig. 3. AOAs for different transmitter–receiver configurations.

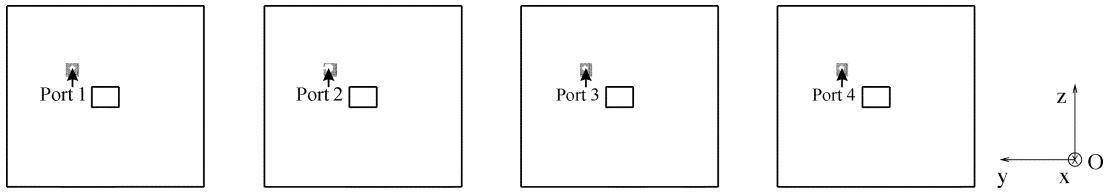

Fig. 4. Four-element HiperLAN patch array.

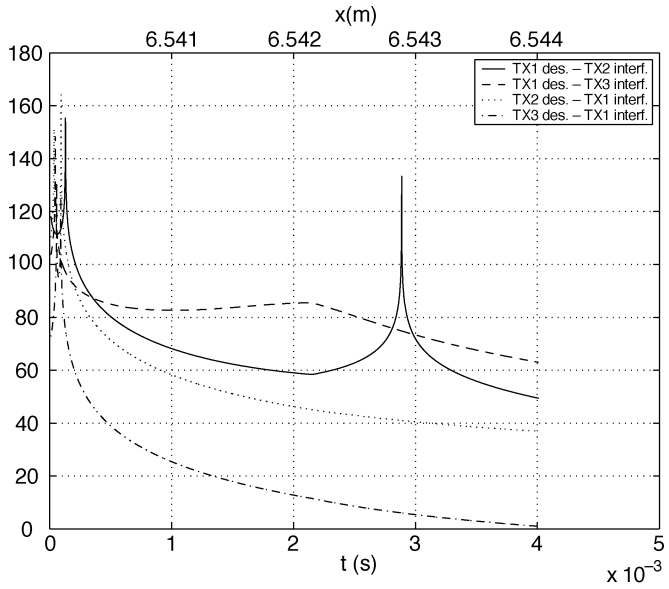

Fig. 5. SIR (decibels) for different desired-transmitter/interferer combinations.

the array training due to the movement of the receiver, a few bit errors (23 bit errors out of 400 transmitted bits) occur when detecting the signal coming from TX3. Indeed, because the array is badly positioned to detect signals coming from TX3, a large amplification is required, making the detection more sensitive to noise.

B. Effect of Training and Tracking

In order to make the detection of the desired signal from TX3 less sensitive to motion of the receiver, we again use the first 16 b of the desired signal as a training sequence known to the receiver. This is now combined with the estimates of the desired bit sequence for tracking at subsequent time instances to calculate the array weights, following (5) and (6). In Fig. 7, the SIR is shown for TX1 as the desired transmitter and TX2 as the interfering source. Note that the time instance $t = 0$ corresponds to the receiver located at the position ($x = 6.54$ m, $y = 3$ m), as in Fig. 2. The SIR is highly oscillating, but its average value of 98 dB does not change much over time. Other transmitter–interferer combinations show a similar SIR behavior, with an average SIR value of 97 dB for TX1 the desired and TX3 the interfering transmitter, 98 dB for TX2 the desired and TX1 the interfering transmitter, and 72 dB for TX3 the desired and TX1 the interfering transmitter. Again, for the last combination, the average SIR is clearly lower than for the previous ones, as can also be seen in Fig. 7.

When white Gaussian noise is added at the receiver with a SNR $= 10$ dB, the array remains able to track the desired bit sequence coming from transmitters TX1 and TX2. However, the array looses tracking when detecting the signal coming from TX3 and locks to the signal coming from TX1. This is seen in Fig. 8, representing the signal-to-noise-plus-interference ratio (SNIR) defined as the ratio of the received power of the desired signal to the received power of the noise-plus-interfering signals. In all cases, the SNIR is highly oscillating, but its average value again does not change much over time. The average SNIR is 25 dB for TX1 the desired and TX2 the interfering transmitter, 30 dB for TX1 the desired and TX3 the interfering transmitter, and 24 dB for TX2 the desired and TX1 the interfering transmitter. Note that the array is able to maintain its lock on transmitter TX3, when the noise level is reduced to SNR $= 20$ dB.

We now increase the receiver speed to 10 m/s. At that speed, the position of the receiver changes by 4 cm during the time required to capture the 400-b sequences emitted by the desired transmitter and receiver. When the array weights are calculated with the 16-b training sequence without tracking, destructive interference between signals at the different array branches occurs quite quickly

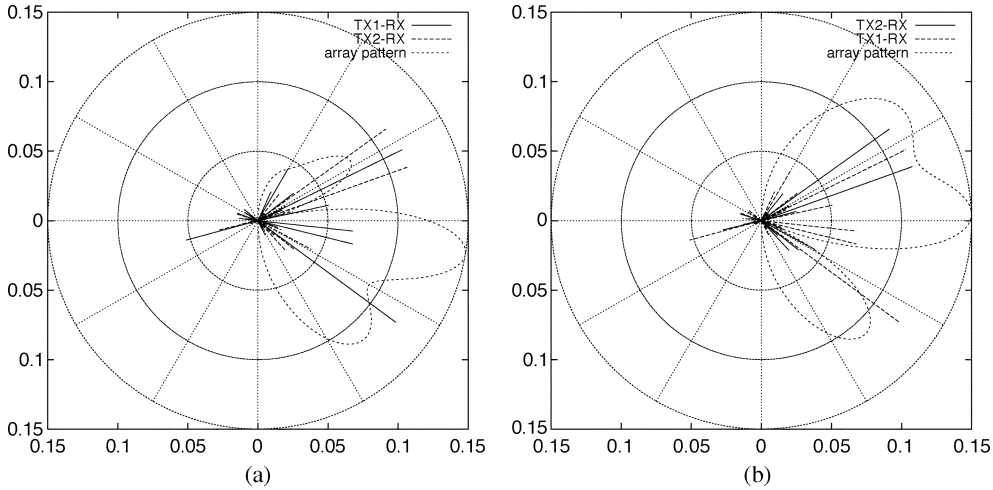

Fig. 6. Radiation pattern after training for (a) TX1 desired and TX2 interferer and for (b) TX2 desired and TXa interferer.

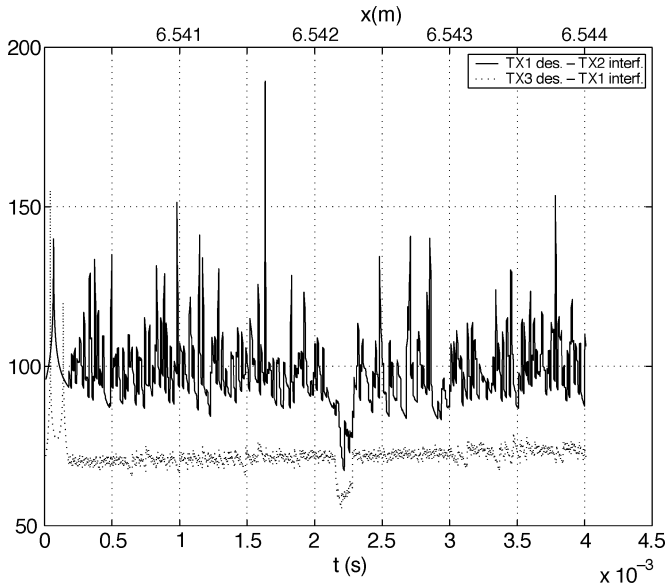

Fig. 7. SIR in decibels for different desired-transmitter/interferer combinations.

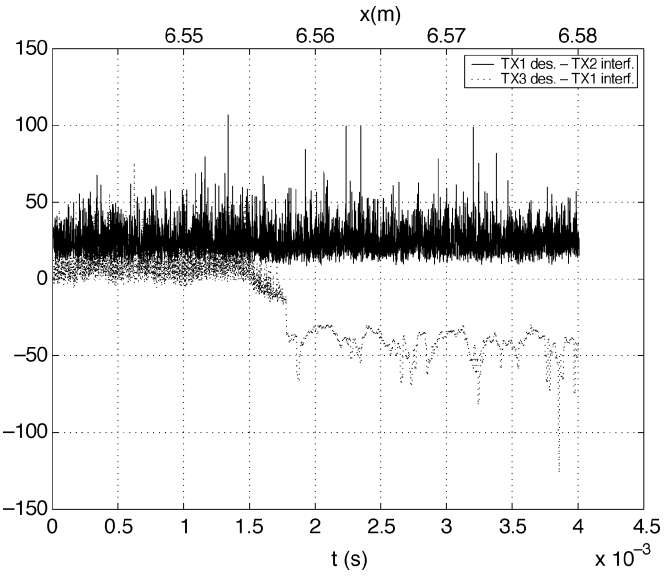

Fig. 8. SNIR in decibels for different desired-transmitter/interferer combinations.

after training, because of the rapid movement of the receiver, resulting in outage and a large number of bit errors because of inadequate training. It is better to continue tracking the channel after training. In the presence of noise, the desired signal coming from TX1 can still be detected for an SNR $= 10$ dB, while the desired signal coming from TX3 can be detected for an SNR $= 20$ dB. Finally, we were able to track a 2000-b sequence coming from TX1 in the presence of noise (SNR $= 10$) dB and interferer TX3. While receiving the 2000-b sequence, the receiver moved over a distance of 20 cm. This shows that the combination of training and tracking allows to suppress interference and noise by adapting to a moving receiver. Since the time between two different training sequences can be relatively high, we avoid degrading the bit rate by creating too much overhead.

IV. Conclusion

We have evaluated the use of a compact smart-antenna system located at the receiver, operating in indoor environments. We have therefore combined the exact active element pattern method to evaluate the electromagnetic field behavior of the compact array with a 2-D ray-tracing approach to describe the channel characteristics of the indoor environment and with training and tracking algorithms to control the amplitude and phase of the array weights. In the ray-tracing approach, it was assumed that the receiver moved around in the indoor environment at a constant speed. It was shown that the combination of training and tracking allowed to detect an omnidirectional desired transmitter in a stable manner, even in the presence of a strong interfering source and noise and for high speeds of the receiver. As the number of elements in the compact array remains low, the training and tracking algorithm are computationally inexpensive and can be evaluated in real time for bit rates up to 2 Mb/s. The theoretical tools developed in this contribution can be of great help for designing practical smart-antenna systems. The formalism can be used to design the optimal interval between training sequences, taking into account the movement of the receiver, the adaptation speed of the tracking algorithm, the required BER, and the reduction in bit rate because of the training sequences.

REFERENCES

[1] H. Nikookar and H. Hashemi, "The indoor radio propagation channel," *Proc. IEEE*, vol. 81, no. 7, pp. 943–968, July 1993.

[2] S.-C. Kim, H. L. Bertoni, and M. Stern, "Pulse propagation characteristics at 2.4 GHz inside buildings," *IEEE Trans. Veh. Technol.*, vol. 45, no. 3, pp. 579–592, Aug. 1996.

[3] M. S. Varela and M. G. Sánchez, "RMS delay and coherence bandwidth measurements in indoor radio channels in the UHF band," *IEEE Trans. Veh. Technol.*, vol. 50, no. 2, pp. 515–525, Mar. 2001.

[4] J. Kivinen, X. Zhao, and P. Vainikainen, "Empirical characterization of wideband indoor radio channel at 5.3 GHz," *IEEE Trans. Antennas Propag.*, vol. 49, no. 8, pp. 1192–1203, Aug. 2001.

[5] I. Cuiñas and M. G. Sánchez, "Measuring, modeling and characterixing of indoor radio channel at 5.8 GHz," *IEEE Trans. Veh. Technol.*, vol. 50, no. 2, pp. 526–535, Mar. 2001.

[6] H. L. Bertoni, W. Honcharenko, J. L. D. L. R. Maciel, and H. H. Xia, "UHF propagation prediction for wireless personal communications," *Proc. IEEE*, vol. 82, no. 9, pp. 1333–1359, Sep. 1994.

[7] H.-J. Li, M.-L. Lee, and R.-Y. Lane, "ISI simulation for indoor wireless communications," *IEEE Trans. Veh. Technol.*, vol. 49, no. 2, pp. 413–421, Mar. 2000.

[8] J.-Y. Lee and H. Samueli, "Adaptive antenna arrays and equalization techniques for high bit-rate QAM receivers," *IEEE J. Sel. Areas Commun.*, vol. 17, no. 4, pp. 677–688, Apr. 1999.

[9] W. Honcharenko, H. L. Bertoni, J. L. Dailing, J. Qian, and H. D. J. Yee, "Mechanisms governing UHF propagation on single floors in modern office buildings," *IEEE Trans. Veh. Technol.*, vol. 41, no. 4, pp. 496–504, Nov. 1992.

[10] J. H. Tarng, W. Chang, and B. J. Hsu, "Three-dimensional modeling of 900-MHz and 2.44-GHz radio propagation in corridors," *IEEE Trans. Veh. Technol.*, vol. 46, no. 2, pp. 519–527, May 1997.

[11] W. Honcharenko, H. L. Bertoni, and J. L. Dailing, "Mechanisms governing UHF propagation on different floors in buildings," *IEEE Trans. Antennas Propag.*, vol. 41, no. 6, pp. 787–790, June 1993.

[12] W. Honcharenko and H. L. Bertoni, "Transmission and reflection characteristics at concrete block walls in the UHF bands proposed for future PCS," *IEEE Trans. Antennas Propag.*, vol. 42, no. 2, pp. 232–239, Feb. 1994.

[13] B. de Backer, H. Börjeson, D. De Zutter, and F. Olyslager, "Propagation mechanisms for UHF wave transmission through walls and windows," *IEEE Trans. Veh. Technol.*, vol. 52, no. 5, pp. 1297–1307, Sep. 2003.

[14] S. H. Chen and S. K. H. Jeng, "An SBR/image approach for radio wave propagation in indoor environments with metallic furniture," *IEEE Trans. Antennas Propag.*, vol. 45, no. 1, pp. 98–106, Jan. 1994.

[15] H. Nikookar and H. Hashemi, "Phase modeling of indoor radio propagation channels," *IEEE Trans. Veh. Technol.*, vol. 49, no. 2, pp. 594–606, Mar. 2000.

[16] H. Rogier and D. De Zutter, "Beamforming strategies for compact arrays using the exact active element pattern method," *Microwave Opt. Technol. Lett.*, vol. 35, pp. 202–203, 2002.

[17] G. Vermeeren, H. Rogier, F. Olyslager, and D. De Zutter, "A low-cost planar rectangular ring antenna for operation in the HiperLAN band," *Electron. Lett.*, vol. 38, pp. 208–209, 2002.

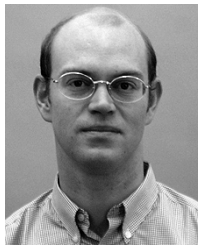

Hendrik Rogier (S'96–A'99–M'00) was born in 1971. He received the degree in electrical engineering in 1994 and the Ph.D. degree in 1999, both from Ghent University, Ghent, Belgium.

He is currently working in the Department of Information Technology, Ghent University, as a Part-Time Profressor and Postdoctoral Fellow of the Fund for Scientific Research in Flanders (FWO-V). He has authored and coauthored approximately 20 papers in international journals and approximately 25 contributions in conference proceedings and has one patent pending. His current research interests include the analysis of electromagnetic waveguides and electromagnetic simulation techniques applied to EMC and signal integrity problems, as well as indoor propagation and antenna design and smart antenna systems for wireless networks.

Dr. Rogier received the URSI Young Scientist Award at the 2001 URSI Symposium on Electromagnetic Theory and at the 2002 URSI General Assembly.

Daniël De Zutter (M'92–SM'96–F'01) was born in 1953. He received the M.Sc. degree in electrical engineering from Ghent University, Ghent, Belgium, in 1976 and received the Ph.D. degree in 1981 and completed a thesis leading to a degree equivalent to the French Aggrégation or the German Habilitation in 1984.

From 1976 to 1984, he was a Research and Teaching Assistant at the same university. From 1984 to 1996, he was with the National Fund for Scientific Research of Belgium. He currently is a Full Professor of electromagnetics and Dean of the Faculty of Engineering at Ghent University. He has authored or co-authored more than 110 international journal papers and 140 papers in conference proceedings. In 1993, he published a book entitled *Electromagnetic and Circuit Modelling of Multiconductor Transmission Lines* (with N. Faché and F. Olyslager) in the Oxford Engineering Science Series. Most of his earlier scientific work dealt with the electrodynamics of moving media. His research now focusses on all aspects of circuit and electromagnetic modeling of high-speed and high-frequency interconnections and packaging, on electromagnetic compatibility (EMC), and numerical solutions of Maxwell's equations.

Dr. De Zutter received the 1990 Montefiore Prize from the University of Liège and the 1995 IEEE Microwave Prize Award (with F. Olyslager and K. Blomme) from the IEEE Microwave Theory and Techniques Society for best publication in the field of microwaves for the year 1993. In 1990, he was elected Member of the Electromagnetics Society. In 1999, he received the Transactions Prize Paper Award from the IEEE EMC Society.